

Probing the peripheral self-generated magnetic field distribution in laser-plasma magnetic reconnection with Martin—Puplett interferometer polarimeter

Ya-Peng Zhang(张雅芃), Jia-Wen Yao(姚嘉文), Zheng-Dong Liu(刘正东), Zuo-Lin Ma(马作霖), and Jia-Yong Zhong(仲佳勇)

Citation: Chin. Phys. B, 2024, 33 (**4**): 045206. DOI: 10.1088/1674-1056/ad24db
Journal homepage: http://cpb.iphy.ac.cn; http://iopscience.iop.org/cpb

What follows is a list of articles you may be interested in

Three-dimensional magnetic reconnection in complex multiple X-point configurations in an ancient solar-lunar terrestrial system

Xiang-Lei He(何向磊), Ao-Hua Mao(毛傲华), Meng-Meng Sun(孙萌萌), Ji-Tong Zou(邹继同), and Xiao-Gang Wang(王晓钢)
Chin. Phys. B, 2024, 33 (**3**): 035202. DOI: 10.1088/1674-1056/ad0b02

Effect of the magnetization parameter on electron acceleration during relativistic magnetic reconnection in ultra-intense laser-produced plasma

Qian Zhang(张茜), Yongli Ping(平永利), Weiming An(安维明), Wei Sun(孙伟), and Jiayong Zhong(仲佳勇)
Chin. Phys. B, 2022, 31 (**6**): 065203. DOI: 10.1088/1674-1056/ac3397

Electron acceleration during magnetic islands coalescence and division process in a guide field reconnection

Shengxing Han(韩圣星), Huanyu Wang(王焕宇), and Xinliang Gao(高新亮)
Chin. Phys. B, 2022, 31 (**2**): 025202. DOI: 10.1088/1674-1056/ac21c0

Spontaneous growth of the reconnection electric field during magnetic reconnection with a guide field: A theoretical model and particle-in-cell simulations

Kai Huang(黄楷), Quan-Ming Lu(陆全明), Rong-Sheng Wang(王荣生), Shui Wang(王水)
Chin. Phys. B, 2020, 29 (**7**): 075202. DOI: 10.1088/1674-1056/ab8da0

Formation of electron depletion layer and parallel electric field in the separatrix region of anti-parallel magnetic reconnection

Zisheng Li(李子圣), Huanyu Wang(王焕宇), Xinliang Gao(高新亮)
Chin. Phys. B, 2019, 28 (**7**): 075203. DOI: 10.1088/1674-1056/28/7/075203

INSTRUMENTATION AND MEASUREMENT

Probing the peripheral self-generated magnetic field distribution in laser-plasma magnetic reconnection with Martin–Puplett interferometer polarimeter

Ya-Peng Zhang(张雅芃)[1,2], Jia-Wen Yao(姚嘉文)[1,2], Zheng-Dong Liu(刘正东)[1,2], Zuo-Lin Ma(马作霖)[1,2], and Jia-Yong Zhong(仲佳勇)[1,2,†]

[1] *Department of Astronomy, Beijing Normal University, Beijing* 100875, *China*
[2] *Institute for Frontiers in Astronomy and Astrophysics, Beijing Normal University, Beijing* 102206, *China*

(Received 24 December 2023; revised manuscript received 30 January 2024; accepted manuscript online 1 February 2024)

Magnetic reconnection of the self-generated magnetic fields in laser-plasma interaction is an important laboratory method for modeling high-energy density astronomical and astrophysical phenomena. We use the Martin–Puplett interferometer (MPI) polarimeter to probe the peripheral magnetic fields generated in the common magnetic reconnection configuration, two separated coplanar plane targets, in laser-target interaction. We introduce a new method that can obtain polarization information from the interference pattern instead of the sinusoidal function fitting of the intensity. A bidirectional magnetic field is observed from the side view, which is consistent with the magneto-hydro-dynamical (MHD) simulation results of self-generated magnetic field reconnection. We find that the cancellation of reverse magnetic fields after averaging and integration along the observing direction could reduce the magnetic field strength by one to two orders of magnitude. It indicates that imaging resolution can significantly affect the accuracy of measured magnetic field strength.

Keywords: laser-plasma experiment, polarimeter, self-generated magnetic field, magnetic reconnection

PACS: 52.38.Fz, 52.70.Kz, 52.35.Vd **DOI:** 10.1088/1674-1056/ad24db

1. Introduction

Self-generated magnetic field research is vital in plasma physics. It exerts an important impact on the physical processes involved with plasmas, such as the movement of ions and electrons, and energy absorption and transport.[1–3] In plasma physics and laboratory astrophysics, the self-generated magnetic field is an important means for constructing magnetic reconnection (MR) configurations for experimental research. MR is associated with the explosive conversion of magnetic energy into plasma kinetic and thermal energies and is thus considered to be a major trigger of eruptive onsets of certain explosive astrophysical events.[4–7] In 2006, Nilson *et al.*[8] first used two approaching laser-created plasmas to model the reconnection geometry in the laboratory. Subsequently, Nilson *et al.*[8] and Li *et al.*[9] definitively proved MR occurred by measuring the magnetic topology changes with the time-resolved proton deflection technique. Using two coplanar plane targets with a gap in between, Dong *et al.*[10] investigated the structure of collisionless reconnection of the self-generated magnetic fields in laser-target interaction. Ping *et al.*[11] demonstrated turbulent magnetic reconnection in laser-generated plasmas created when irradiating solid targets and reproduced the key features of solar flare observations.[12,13]

In laser-plasma experiments, the commonly used magnetic field detection methods are proton photography[14] and magnetic probe[15] methods, while the cases of optical diagnostic methods for probing magnetic fields are relatively limited. Here we use the new type of optical polarimeter based on the Martin–Puplett interferometer (MPI)[16] to probe the peripheral self-generated magnetic field distribution in laser-plasma MR. MPI polarimeter is developed for probing magnetic fields with the Faraday rotation method.[17] Utilizing the polarization characteristics of MPI can overcome the depolarization problem of the probe light and the response difference problem of separated images in traditional diagnostic methods. According to Eqs. 2.3–2.5 in Zhang *et al.* (2023),[16] the resulting intensity after interference is determined by the phase difference and the polarization angle. For each pixel at a fixed position, the intensity varies as a sinusoidal function of the polarization angle. Therefore, the signal polarization direction can be calculated by fitting the sinusoidal function.

In this paper, we provide another method for calculating the polarization angle with the MPI polarimeter. This method does not use sinusoidal function fitting but uses the interference pattern to obtain polarization information. In Section 2, we demonstrate the principle of the new method for solving the polarization. We use simulated data to display the calculation results. In Section 3, we use this method to probe the peripheral magnetic fields generated in laser–target interaction by using two separate coplanar plane targets. And we compare

†Corresponding author. E-mail: jyzhong@bnu.edu.cn

© 2024 Chinese Physical Society and IOP Publishing Ltd

the measured result with 3D FLASH simulation. Section 4 is the summary.

2. How to measure polarization direction with MPI

MPI optical polarimeter is designed based on the polarizing interferometer invented by Martin and Puplett,[18] which is also a special type of Michelson interferometer. In an MPI, the main components include 2 polarizers and 2 roof mirrors. One polarizer is used for splitting the incident light into two beams with polarization perpendicular to each other. The other one is on the output side to ensure the output beams from the two arms are in the same polarization direction. It is situated with the polarization direction at 45° from the beam splitter so that the proportion of residual components is the same for the two beams. The two roof mirrors reflect the two beams and make them can be combined when they come back to the splitter.

By setting the length difference between the two arms equal to one-fourth of the wavelength, the optical path difference is equal to half of the wavelength. In this way, the two paths of light meet the phase condition of destructive interference. After interference, the output intensity is not affected by the nonpolarized component and is related to the intensity and direction of linearly polarized light.

In most cases of laser-plasma experiments, the probe beam needs to pass through all imaging lenses and prisms before reaching the detectors. Therefore, the light does not propagate in the form of an ideal plane wave. This results in fringes of equal inclination interference, which is described by Eq. 2.5 in Zhang *et al.* (2023)[16]

$$\begin{aligned} I_{\text{out}} &= I\sin^2(\theta) + I\cos^2(\theta) + 2I\sin(\theta)\cos(\theta)\cos(\Delta\varphi) \\ &= I[1 + 2\sin(\theta)\cos(\theta)\cos(\Delta\varphi)]. \end{aligned}$$

The detected output intensity is a sinusoidal function of polarization direction. We can use the fitted function to calculate the signal polarization direction in the experiment.

2.1. Calculating the polarization angle from the interference pattern

From Eq. 2.5 in Zhang *et al.* (2023),[16] we can find that the intensity of interference fringes obtained after the MPI polarimeter depends on (i) the polarization direction of the input probe light θ and (ii) the phase difference at each CCD pixel $\Delta\varphi$. For the polarized light at a specific angle, i.e., θ is fixed, the intensity at a specific pixel is fixed. Since the result of interference is a pattern of equal inclination interference, the intensities of the pixels at different positions are also correlated.

We plot Eq. 2.5 in Fig. 1 with polarization angle θ and phase difference $\Delta\varphi$ as variables. From Fig. 1, it can be intuitively seen that the light intensity after interference not only exhibits periodic changes with polarization angle but also changes periodically with phase difference. Since the intensities of the pixels at different positions are correlated, the interference results will exhibit specific stripes when the polarization angle is determined.

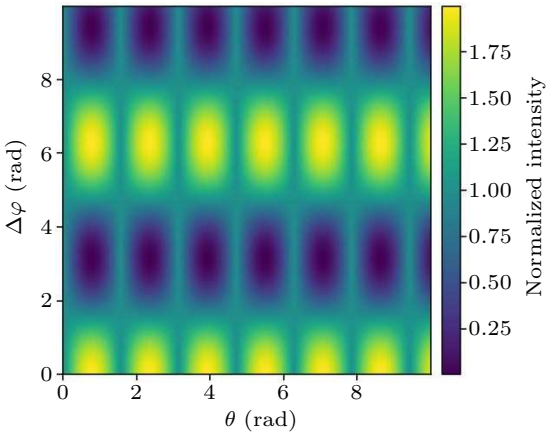


Fig. 1. The 2D plot of Eq. 2.5 in Zhang *et al.* (2023).[16] The intensity is normalized in this plot. The intensity changes periodically with both polarization angle θ and phase difference $\Delta\varphi$.

In real-life experiments, the fringes of equal inclination interference are not uniformly distributed. Nevertheless, we can still find the same pattern for calculating the polarization angle. Figure 2 is an example of equal inclination interference fringes, which have the following characteristics.

(i) The center level of the stripe is high, while the edge level is low.

(ii) The stripe at the center is sparse, and the edge stripe is dense.

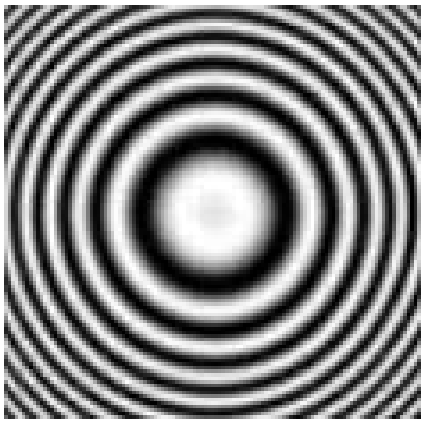


Fig. 2. A schematic diagram of the equal inclination interference stripe.

Based on the characteristics of equal inclination interference fringes, we can find that there is an intensity change from the center of the fringes radially outward. Even if the width of the stripes is different, the amplitude of their brightness change still varies with the polarization angle. Therefore, we can obtain the relationship between polarization angle and amplitude by collecting background images and fitting the intensity change curves.

2.2. Simulation study

To further demonstrate the variation of fringes with incident polarization angle under equal inclination interference, we simulate the imaging situation of the MPI polarimeter with ZEMAX. The *XY* plane schematic diagram of the simulation setup is shown in Fig. 3. The *Z*-axis direction is perpendicular to the paper surface and outward.

The simulation is set according to the MPI polarimeter. The beam-splitting polarizer is placed at 45° to the probe beam. And its polarization axis is at 45° to the *Z*-axis. The 2 roof mirrors control the optical path difference between the two arms. The analyzing polarizer has a polarization axis parallel to the *Z*-axis. In addition, to mimic the optical path situation in the optical diagnosis of laser-plasma experiments, we also add a lens in the simulation.

By changing the polarization direction of the incident light, we obtain the imaging performance of the MPI polarimeter when the probe beam carries polarization in different directions. The imaging results are shown in Fig. 4.

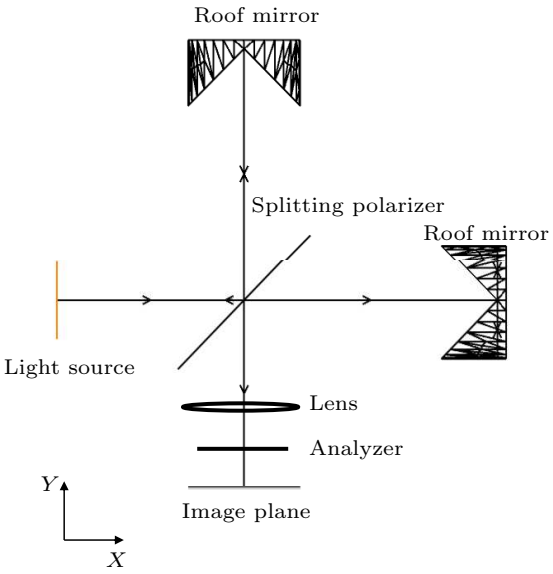


Fig. 3. The schematic diagram of the ZEMAX simulation setup.

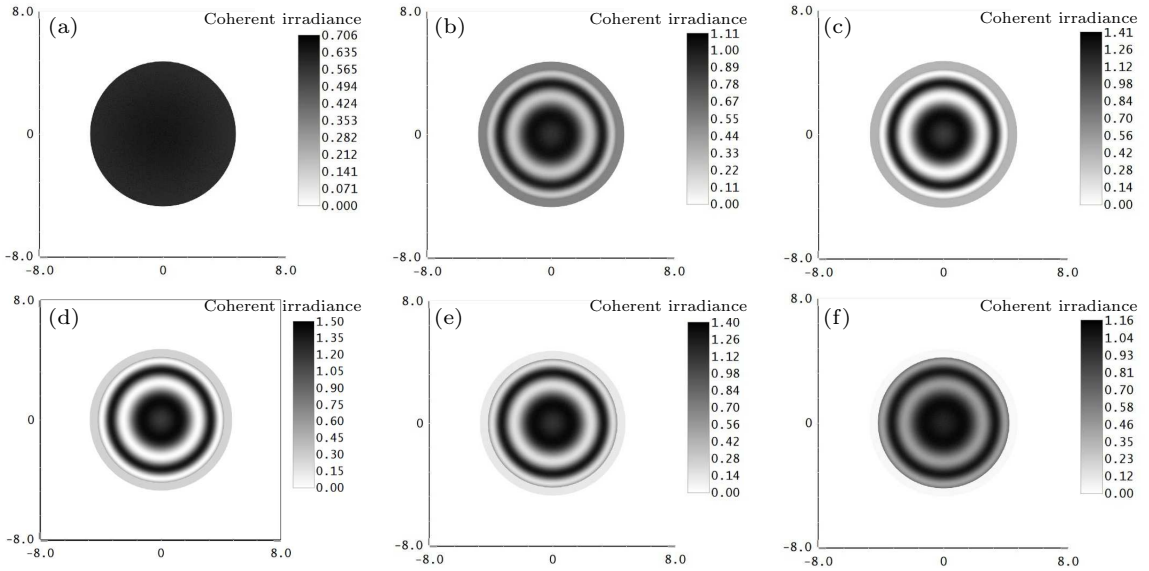


Fig. 4. The ZEMAX simulation results of the MPI polarimeter for different input polarization directions. From panels (a) to (f), the polarization directions are 45°, 60°, 75°, 90°, 105°, and 120° from the *Z*-axis.

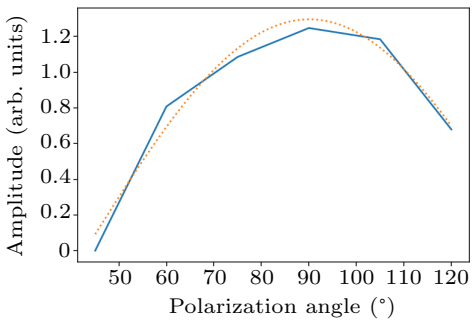


Fig. 5. The relationship between amplitude and polarization angle. The orange dot line is the fitted curve.

From the simulation results, we find that when the polarization direction is parallel or perpendicular to the *Z*-axis, i.e., 45° from the polarization axis of the beam-splitting polarizer, the interference fringes have the largest amplitudes. As the polarization angle rotates, the brightness difference between the bright and dark rings gradually decreases, and the amplitude of the interference fringes also decreases. When the polarization direction is parallel or perpendicular to the polarization axis of the beam-splitting polarizer, the interference fringes disappear. This is because, in this case, only one arm of the MPI has the signal and cannot interfere.

The relationship between amplitude and polarization angle can be known through simulation results. Due to the central symmetry of the interference fringes, we select the cross-section along the *X*-axis to obtain the intensity curve and calculate the amplitudes. We plot the amplitudes at each polarization direction in Fig. 5. By fitting the curve, we obtain that

amplitude changes Amp is

$$\text{Amp} = 1.20 \times \sin(0.035 \times \theta + 90.17) + 0.09,$$

and the *R*-square equal to 0.97.

3. Studying the peripheral self-generated magnetic field in MR

3.1. Experimental result

The experiment was performed at the Shenguang II (SG-II) laser facility in the National Laboratory on High Power Laser and Physics. The SG-II laser facility has eight laser beams and each beam can deliver 250 J of energy in 1 ns square pulse. Figure 6 is a schematic diagram of the experiment setup. We used two laser beams to form a bunch in the experiment. Two synchronized laser bunches were focused onto two Al foil targets from the same side. Each bunch was focused to a focal spot diameter of 150 μm full width at half maximum (FWHM), giving an incident laser intensity of about 10^{15} W/cm^2. The distance between the focal spots was 900 μm. The two Al foil targets were juxtaposed in the same plane and separated by 600 μm. Each Al plate is $900 \times 600 \times 100$ μm in size.

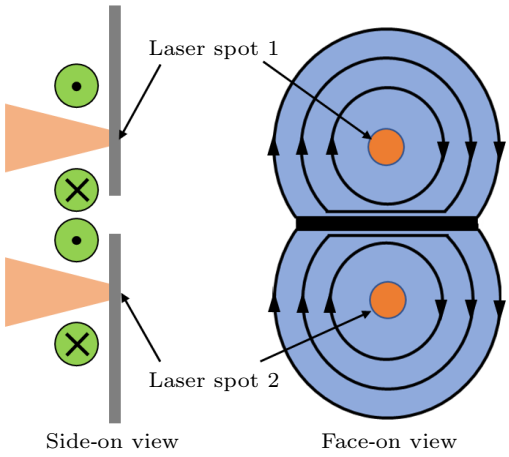


Fig. 6. Experiment setup and magnetic field configurations.

The direction of the optical diagnosis perspective is the side-on view. The MPI polarimeter diagnoses the magnetic field with a short pulse (60 ps) probe beam at 527 nm. The magnification is 2.4 and the resolution is 5.5 μm. According to the Faraday effect, the measured magnetic field is the component along the beam propagation direction. In Fig. 7, panel (a) shows the reference image collected before laser shooting. Panel (b) is the experimental results taken at a delay of 2 ns to the front of the laser pulse. From panel (a), it can be seen the equal inclination interference circular interference fringes imaged by the MPI polarimeter. In panel (b), due to the high density of the plasma, the central region of the interference fringes is blocked. And through the optical probe, the internal structures of the plasma are overlapped after integration, which makes it very difficult to diagnose. Therefore, we select the peripheral area for research.

When analyzing the peripheral plasma in the red arc-shaped region, we divided the region equally into 10 areas. The center of the interference rings is set as the origin of polar coordinates. For each area in Figs. 7(a) and 7(b), we averaged the intensity at the same radius and obtained the intensity-radius relation in each area. Then we used curve-fit code from scipy and got the amplitudes. According to the method in Section 2, we calculated the corresponding amplitude change in each area. Based on the relationship between amplitude change and polarization direction rotation, the changes in polarization angle obtained from top to bottom for the 10 regions are –0.75°, –1.12°, –2.71°, –1.31°, 0.87°, –0.58°, 0.02°, 2.22°, 1.25°, and –0.25°. Calculating with the simulation result and estimated plasma density of 10^{19} cm^{-3}, the corresponding magnetic field intensity is about the order of 0.1 T. Previous studies showed that magnetic field generated in hot, high-density plasmas by irradiating a solid target using high-power laser beams can reach 10 T.[8] The measured magnetic field is pretty lower than expected.

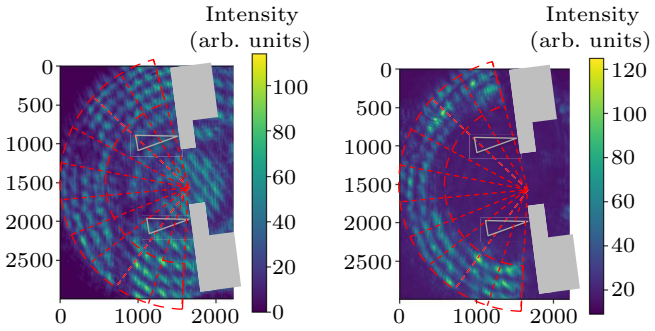


Fig. 7. Probe beam images of the MPI polarimeter in SG-II laser-plasma MR experiment. Panel (a) is the reference image obtained before the laser shooting and panel (b) is at a delay of 2 ns to the front of the laser pulse.

3.2. Simulation

To study the issue of the measured low-strength self-generated magnetic field in the MR experiment, we simulate it with FLASH code using the same parameters as the experiment. The laser-driven MR process can be reasonably described by MHD simulation. Figure 8(a) is the central slice of the magnetic field component along the observation direction at 2 ns. And Fig. 8(b) is the averaged magnetic field after integration. The peripheral magnetic field, generated by the Biermann battery effect, expands forward with the plasma surface with a velocity of approximately 1200 km/s. The strength of the magnetic field component along the direction of the probe beam reaches 3 T. However, after integration along the direction of optical diagnosis, the maximum magnetic field strength is only about 0.4 T. Through this analysis, we find that after integration, the observed magnetic field will decrease by

an order of magnitude. This because magnetic fields are vectors, and reverse magnetic fields cancel out each other. Therefore, the more symmetrical the magnetic field structure is, the greater the measurement errors it will result in.

There are also other factors like probe beam attenuation, scattering, instrumentation sensitivity, or plasma effects that could influence the results of magnetic field diagnosis. As summarized by Zaraś-Szydłowska *et al.* (2020), three main factors reduce the accuracy of magnetic field measurement with the Faraday rotation method: (i) depolarization of the probe beam, (ii) inhomogeneity of the probe beam, and (iii) influence of parasitic plasma self-luminosity.[18] Among them, factors (ii) and (iii) are usually reduced by taking reference images and using narrow-band filters. And their effects are well controlled. Factor (i) is mainly caused by scattering and refraction due to the plasma density and temperature gradients, imperfections in optical elements, and a setup misalignment. This problem is difficult to remove in the traditional Faraday measurements with a linear polarizer or Wollaston prism but can be suppressed by the MPI polarimeter. Because MPI measures the polarization through interference, the unpolarized components can be greatly eliminated. Therefore, the probability of factor (i) producing such a significant impact is relatively low.

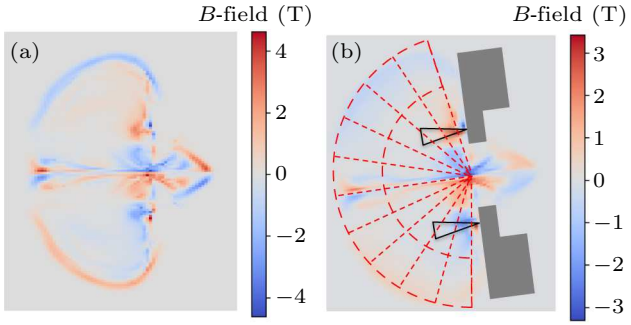


Fig. 8. Simulation results with FLASH code. (a) Middle layer magnetic field. (b) Averaged magnetic field after integration along the observing direction.

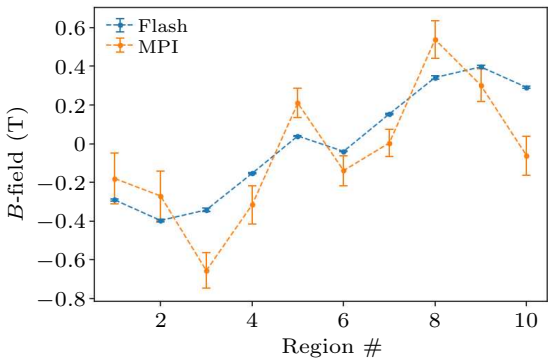


Fig. 9. The simulated (after integration) and measured magnetic field strengths in the 10 regions from top to bottom. The error of the measured result is calculated from the covariance of fitting parameters. The error in FLASH data is the standard error of the average magnetic field in each region.

Due to magnetic reconnection in the interaction region, a reverse magnetic field point is formed at the central position of the peripheral magnetic field. We also divide the integration plot based on the method of processing experimental data. Figure 9 presents both the simulated and measured magnetic field strengths in the 10 regions from top to bottom. The variation trend of the magnetic field in simulation agrees with the experimental results. They are consistent with the configuration structure of the self-generated magnetic field in laser-driven MR.

4. Conclusion and perspectives

We mapped the peripheral magnetic field in the laser-driven MR experiment with the MPI polarimeter. We used the data processing method which utilizes the relationship between the changes in interference fringes and the polarization angle to obtain polarization information from the measured fringes. We obtained the bidirectional structure magnetic field which is consistent with the FLASH simulation. The measured magnetic field strength is one to two orders of magnitude smaller than expected. This is likely because of the cancellation of reverse magnetic fields after averaging and integration along the observing direction. This result indicates that imaging resolution has a significant impact on accurately measuring magnetic fields.

Acknowledgments

We are very grateful to the staff of the Shenguang Laser facility in Shanghai and the colleagues in LARG at Beijing Normal University for their support.

Project supported by the National Key R&D Program of China (Grant Nos. 2022YFA1603200 and 2022YFA1603203), the National Natural Science Foundation of China (Grant Nos. 12075030, 12135001, 12175018, and 12325305), the Strategic Priority Research Program of the Chinese Academy of Sciences (Grant No. XDA25030700), the Research Grants Council of Hong (Grant No. 14307118), and the Youth Interdisciplinary Team (Grant No. JCTD-2022-05).

Y. Z. is supported by the China Postdoctoral International Exchange Program.

References

[1] Stamper J A 1991 *Laser Part. Beams* **9** 841
[2] Lindl J D, Amendt P, Berger R L, *et al.* 2004 *Phys. Plasmas* **11** 339
[3] Schurtz G, Gary S, Hulin S, *et al.* 2007 *Phys. Rev. Lett.* **98** 095002
[4] Sweet P A 1958 *Int. Astron. Union Symp.* **6** 123
[5] Parker E N 1957 *J. Geophys. Res.* **62** 509
[6] Sych R, Nakariakov V M, Karlicky M, *et al.* 2009 *Astron. Astrophys.* **505** 791
[7] Gosling J T, Phan T D, Lin R P, *et al.* 2007 *Geophys. Res. Lett.* **34** 15110
[8] Nilson P M, Willingale L, Kaluza M C, *et al.* 2006 *Phys. Rev. Lett.* **97** 255001

[9] Li C K, Seguin F H, Frenje J A, *et al.* 2007 *Phys. Rev. Lett.* **99** 055001
[10] Dong Q L, Wang S J, Lu Q M, *et al.* 2012 *Phys. Rev. Lett.* **108** 215001
[11] Ping Y, Zhong J, Wang X, *et al.* 2023 *Nat. Phys.* **19** 263
[12] Pesnell W D, Thompson B J and Chamberlin P C 2012 *Solar Phys.* **275** 3
[13] Fox N J, Velli M C, Bale S D, *et al.* 2016 *Space Sci. Rev.* **204** 7
[14] Borghesi M, Campbell D H, Schiavi A, *et al.* 2002 *Laser Part. Beams* **20** 269
[15] Korobkin V V and Serov R V 1966 *JETP Lett.* **4** 70
[16] Zhang Y, Liu Z, Xing C, *et al.* 2023 *Rev. Sci. Instrum.* **94** 033505
[17] Stamper J A and Ripin B H 1975 *Phys. Rev. Lett.* **34** 138
[18] Martin D H and Puplett E 1970 *Infrared Phys.* **10** 105
[19] Zaraś-Szydłowska A, Pisarczyk T, Chodukowski T, *et al.* 2020 *AIP Adv.* **10** 115201